ELSEVIER

Age-Structured and Two-Delay Models for Erythropoiesis

JACQUES BÉLAIR
Département de Mathématiques et de Statistique and Centre de Recherches Mathématiques, Université de Montréal, Montréal, Québec, Canada H3C 3J7, and Center for Nonlinear Dynamics, McGill University

MICHAEL C. MACKEY
Department of Physiology, Center for Nonlinear Dynamics, McGill University, Montreal, Quebec, Canada H3G 1Y6

AND

JOSEPH M. MAHAFFY
Department of Mathematical Sciences, San Diego State University, San Diego, California 92182

Received 20 January 1994; revised 10 August 1994

ABSTRACT

An age-structured model is developed for erythropoiesis and is reduced to a system of threshold-type differential delay equations using the method of characteristics. Under certain assumptions, this model can be reduced to a system of delay differential equations with two delays. The parameters in the system are estimated from experimental data, and the model is simulated for a normal human subject following a loss of blood. The characteristic equation of the two-delay equation is analyzed and shown to exhibit Hopf bifurcations when the destruction rate of erythrocytes is increased. A numerical study for a rabbit with autoimmune hemolytic anemia is performed and compared with experimental data.

1. INTRODUCTION

A number of pathophysiological conditions are marked by the transition of normally constant physiological quantities to an oscillatory state or the transition of an oscillatory physiological variable to a different pattern of dynamic variation. Such disease states have been called periodic diseases [1].

It has been proposed [2] that many periodic diseases might be due to the operation of an intact physiological control system in a region of parameter space different than normal and characterized by a bifurcation in the underlying system dynamics. Periodic diseases satisfying this

0025-5564/95/$9.50

criterion have been called dynamic diseases [3]. This concept has been successfully employed to explain the dynamic pathology seen in respiratory abnormalities [2, 4], neurological disorders [5–10], various pathologies of cardiac rhythmicity [11–22], and several hematological disorders [23–30] and has been invoked as a qualitative explanation of some periodic psychiatric disorders [31, 32]. All of these studies have exploited the existence of multiple bifurcations in system dynamics in offering an understanding of the underlying pathology. A review of this material and the potential applicability of the concept of dynamical diseases to other pathological states may be found in [33–36].

In this paper we propose a simple model for the regulation of mammalian erythropoiesis and examine its dynamics. We outline in this section the normal architecture of the erythroid production system and the nature of the control mechanisms operating therein. This background is used to motivate the formulation of an age-structured model for erythropoiesis in Section 2 that can exhibit behavior reminiscent of some oscillatory derangements of hemostatis. In Section 3 the method of characteristics is employed to reduce the system of partial differential equations to a system of threshold-type delay equations. We show in Section 4 how, under certain biologically realistic simplifying assumptions, the age-structured erythropoiesis model reduces to a pair of coupled differential delay equations with two distinct time delays. Section 5 contains estimates of the relevant model parameters for erythropoiesis and employs these considerations to numerically examine the dynamical behavior of the model for a normal subject. In Section 6, a local stability analysis of the two-delay system of differential equations is performed. The analysis shows that Hopf bifurcations can occur for certain physiological parameters in the hematopoietic system. A simulation compares this analysis to an experimental case of hemolytic anemia, which showed oscillations in erythrocyte populations. We conclude the paper with a brief discussion in the final section.

REGULATION OF ERYTHROPOIESIS (RED CELL PRODUCTION)

Hematopoiesis is the process by which stem cells, primarily in the bone marrow, differentiate and proliferate to supply the body with erythrocytes (red blood cells), platelets, neutrophils, macrophages, and many other specialized cells. These cells perform a variety of vital functions, such as transporting oxygen, repairing lesions, maintaining clotting capability, and fighting infections; hence, the body must carefully regulate their production. For example, on average each day the body must produce 3×10^9 new erythrocytes for each kilogram of body weight. This need changes if physiological conditions change such as the loss of blood due to a blood donation, a substantial hemorrhage, or

different environmental conditions like high elevation. The body uses a complex system of hormonal controls to regulate these hematopoietic systems.

Figure 1 diagrams the principal elements in erythropoiesis. Details of this regulatory system can be found in Williams [37]. It begins with the pluripotential stem cells that differentiate in one of three ways to produce erythrocytes, platelets, or granulocytes (representing the core line for many different elements of the immune system). The next stage in erythroid development are the burst-forming units (BFU-Es), which is a self-sustaining population of cells that show minimal signs of differentiation but respond to the appropriate hormones to accelerate proliferation in response to physiological needs.

Erythropoietin (Epo) is the hormone that stimulates reproduction of the BFU-Es and causes further differentiation into the colony-forming units (CFU-Es). The CFU-E cell line is apparently not self-sustaining and, after a series of divisions, results in mature erythrocytes or red blood cells. Following the formation of the CFU-Es, there are a series of cell divisions at approximately 8-h intervals for several days with early stages under the control of Epo. In the beginning the cells are rapidly proliferating and produce proerythroblasts, basophilic erythroblasts, etc. These stages are differentiated by increasing levels of hemoglobin, the component of red blood cells that gives them their red color and provides them with their ability to transport oxygen. When the cells

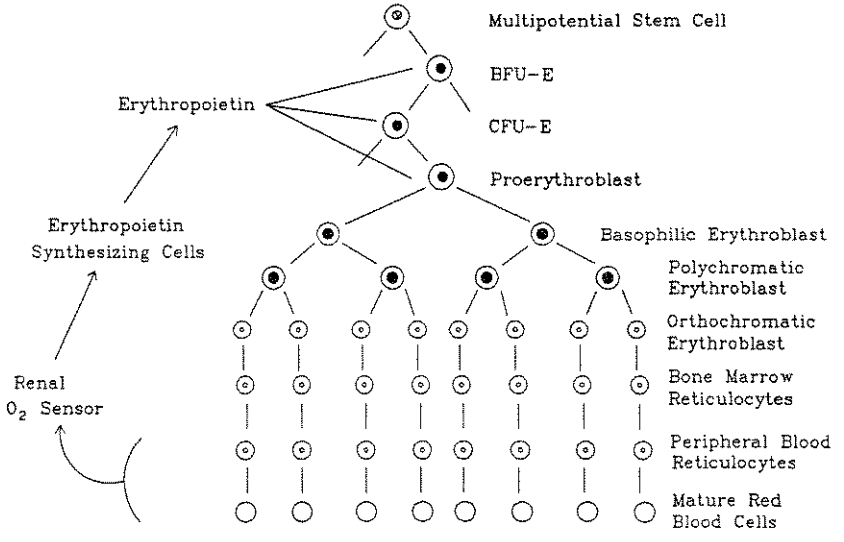

FIG. 1. Diagram of key elements for erythropoiesis.

reach the stage of becoming reticulocytes, they stop dividing and simply mature by increasing their hemoglobin content.

All of the above stages take place primarily in the bone marrow and require about 6 days from the appearance of the CFU-Es to produce peripheral blood reticulocytes. After a certain level of maturity is attained, the reticulocytes migrate to the bloodstream and become part of the circulatory system. Apparently, higher levels of Epo can accelerate the maturing process along with increased proliferation. In the bloodstream the reticulocytes lose their nuclei and become mature erythrocytes, which carry oxygen through the body for about 120 days. The toll on their membrane of passing through hundreds of miles of capillaries without a nucleus to effect repair causes them to become less efficient at carrying oxygen. When the cell membrane loses pliability, the erythrocytes are actively degraded by macrophages (from the granulocyte cell line).

There is a population of cells near the kidneys that respond to levels of oxygen in the blood. When the partial pressure of oxygen drops, these cells release Epo into the bloodstream. Epo circulates through the bone marrow and affects both the recruitment and maturation of the erythrocyte cell line as described above. For fixed environmental conditions, the oxygen content of the blood is directly proportional to the number of erythrocytes circulating in the bloodstream, which links the feedback between Epo and erythrocytes. The hormone erythropoietin has a half-life of only 6 h, so this short-lived hormone creates a rapid response to changing conditions.

2. THE AGE-STRUCTURED MODEL FOR ERYTHROPOIESIS

The discussion above for erythropoiesis describes a situation that, from a modeling perspective, is appropriate for age-structured populations [38–43]. The population of precursor cells matures at differing rates depending on the Epo concentration, which in turn varies according to the oxygen-carrying capacity of the blood. This depends on the mature cells, which also have an age structure. In this section we present a general age-structured model for erythropoiesis.

Let $p(t, \mu)$ be the population of precursor cells that are multiplying and maturing after differentiation from the stem cells. The stem cells (or possibly the self-maintaining BFU-Es) become committed to maturing into erythrocytes based on the level of Epo in the bloodstream. The precursor cell population consists of the proliferating BFU-Es, the CFU-Es, proerythroblasts, erythroblasts, and reticulocytes. The variable t represents time, while μ represents the maturity level of this pool of

cells. For erythrocytes, the variable μ might represent the hemoglobin content within the cell. $E(t)$ is the hormone level, which for erythropoiesis is primarily erythropoietin. In general, the rate of maturation of the precursor cells seems to be affected by the level of E, with higher concentrations accelerating the maturing process somewhat. Thus, the velocity of maturing, $V(E)$, increases with E.

Let $m(t, \nu)$ be the population of mature nonproliferating cells at time t and age ν. Assume that the mature cells age at a rate W, which is considered to be a constant for erythropoiesis as the aging process appears to depend only on the number of times that an erythrocyte passes through the capillaries. The total population of mature cells, $M(t)$, determines the level of the hormone, E. The concentration E decreases with increasing numbers of mature erythrocytes, representing a negative feedback. Figure 2 presents a schematic representation for the age-structured model of erythropoiesis.

Let $S_0(E)$ be the number of cells recruited into the proliferating precursor population. The function S_0 depends on the hormone level E and is probably some type of saturation function. The new precursor cells enter the age-structured model by the boundary condition

$$V(E)p(t,0) = S_0(E). \tag{2.1}$$

When the cells achieve a certain level of maturity, they are released into the bloodstream as mature cells. Let $h(\mu - \overline{\mu})$ be the distribution

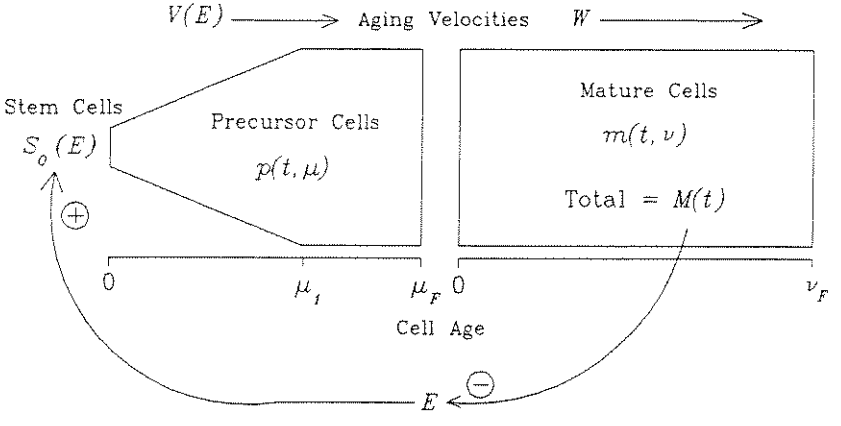

FIG. 2. Schematic representation for an age-structured model of erythropoiesis.

of maturity levels of the cells when released into the circulating blood, where $\bar{\mu}$ represents the mean age of mature precursor cells and

$$\int_0^{\mu_F} h(\mu - \bar{\mu})\, d\mu = 1.$$

With this assumption the boundary condition for cells entering the mature population is given by the expression

$$Wm(t,0) = \int_0^{\mu_F} h(\mu - \bar{\mu})\, p(t,\mu)\, d\mu, \tag{2.2}$$

where the maturity level μ_F represents the maximum age for a cell at maturity.

For proliferating precursor cells, the net birth rate is assumed to be $\beta(\mu, E)$, which depends on both the maturity of the cell and the level of hormone E. The precursor cells rapidly divide early in the maturation process, then stop replicating totally when they reach the reticulocyte stage. Past this point they synthesize hemoglobin in preparation for release into the bloodstream as mature erythrocytes. To include the maturing of precursor cells in the age-structured model, we follow the techniques of Metz and Diekmann [43] and Webb [44]. From the boundary condition (2.2), we introduce the disappearance rate function

$$H(\mu) = \frac{h(\mu - \bar{\mu})}{\int_\mu^{\mu_F} h(s - \bar{\mu})\, ds}.$$

Experimental observations indicate that there is little cell death in the precursor population [45], so no term is included for this. With these assumptions the age-structured model for the precursor cells can be written

$$\frac{\partial p}{\partial t} + V(E)\frac{\partial p}{\partial \mu} = \beta(\mu, E)p - V(E)H(\mu)p, \qquad t > 0;\ 0 < \mu < \mu_F. \tag{2.3}$$

If $\gamma(\nu)$ is the death rate of mature cells depending only on age, then the partial differential equation describing $m(t,\nu)$ is given by

$$\frac{\partial m}{\partial t} + W\frac{\partial m}{\partial \nu} = -\gamma(\nu)m, \qquad t > 0;\ 0 < \nu < \nu_F. \tag{2.4}$$

Note that we are assuming that there is a maximum age for the mature cells, ν_F. An equivalent assumption is that γ becomes infinite for $\nu \geq \nu_F$.

The hormone level E is governed by a differential equation with a negative feedback. Let $M(t)$, the total population of mature cells, be given by

$$M(t) = \int_0^{\nu_F} m(t, \nu) d\nu; \tag{2.5}$$

then the differential equation for E is

$$\frac{dE}{dt} = f(M) - kE, \tag{2.6}$$

where k is the decay constant for the hormone and $f(M)$ is a monotone decreasing function of M (negative feedback). Erythropoietin is removed by the liver through enzymatic degradation, while its release is governed by cells near the kidneys that release Epo when oxygen levels decline. Typically, we shall consider the following form of f:

$$f(M) = \frac{a}{1 + KM^r}, \tag{2.7}$$

which is a Hill function that often occurs in enzyme kinetic problems.

3. REDUCING THE AGE-STRUCTURED MODEL TO A SYSTEM OF THRESHOLD-TYPE DELAY EQUATIONS

The model presented above consists of partial differential equations that describe the age-structured populations of erythrocytes at various stages in their life cycle. These partial differential equations are coupled in a complicated manner to equations governing the dynamics of the controlling hormone erythropoietin. This type of modeling system has been studied by several authors [43, 46–48]. To simplify this system of equations we assume that a solution to (2.6) is known for $E(t)$, then integrate along the characteristics for the partial differential equations (2.3) and (2.4) to find solutions $p(t, \mu)$ and $m(t, \nu)$. Our technique follows the population study of Smith [48], which reduces a system of partial differential equations to a system of threshold delay equations. Details of the calculations are presented in the Appendix.

The method of characteristics is used to simplify the partial differential equations (2.3) and (2.4). First, define the characteristic curve C_0

emanating from the origin in the $t\mu$ plane with $t > 0$ and $0 < \mu < \mu_F$. If we assume that $E(t)$ is known, then the curve C_0 satisfies

$$t(s) = s \qquad \text{and} \qquad \mu(s) = \int_0^s V(E(\sigma))\,d\sigma, \qquad s \in [0, s_F],$$

where s_F is the *threshold value* found by solving

$$\mu_F = \int_0^{s_F} V(E(\sigma))\,d\sigma.$$

This curve C_0 separates the $t\mu$ space into two regions as shown in Figure 3. The region S_1 allows solutions that depend on the initial conditions of the problem, while S_2 is where longer time solutions exist and depends on the boundary conditions imposed. Figure 3 shows typical characteristic curves in each of the regions.

For a given pair of variables $(t, \mu) \in S_2$, a state-dependent delay τ is implicitly defined by the integral

$$\mu = \int_{t-\tau}^{t} V(E(\tau))\,dr. \tag{3.1}$$

This delay represents the time required for the maturation to go from 0 to μ and is found with knowledge of the history of the hormone concentration E.

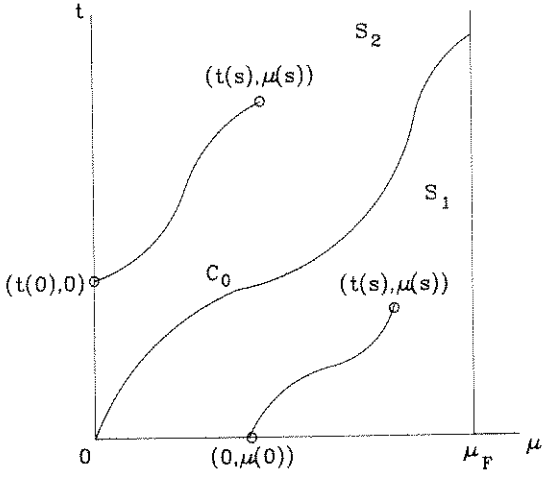

FIG. 3. Characteristic curves parametrized by s in the region $t > 0$ and $0 < \mu < \mu_F$ showing regions S_1 and S_2.

Assume that the initial age structure of the population satisfies

$$p(0,\mu)=\phi(u), \qquad m(0,\nu)=\psi(\nu). \tag{3.2}$$

The method of characteristics, as developed in the Appendix, gives the following solution to the partial differential equation (2.3):

$$p(t,\mu)=\begin{cases}\phi\left(\mu-\int_0^t V(E(r))\,dr\right)\exp\left[\int_0^t\left\{\beta\left(\mu-\int_w^t V(E(r))\,dr,E(w)\right)\right.\right.\\ \qquad\left.\left.-V(E(w))H\left(\mu-\int_w^t V(E(r))\,dr\right)\right\}dw\right], \quad (t,\mu)\in S_1,\\ \dfrac{S_0(E(t-\tau))}{V(E(t-\tau))}\exp\left[\int_{t-\tau}^t\left\{\beta\left(\int_{t-\tau}^w V(E(r))\,dr,E(w)\right)\right.\right.\\ \qquad\left.\left.-V(E(w))H\left(\int_{t-\tau}^w V(E(r))\,dr\right)\right\}dw\right], \quad (t,\mu)\in S_2,\end{cases} \tag{3.2}$$

where τ is determined by the threshold equation (3.1). Since the aging rate of mature cells W is a constant, classical methods may be used to solve (2.4), producing the result

$$m(t,\nu)=\begin{cases}\psi(\nu-Wt)\exp\left[-\int_0^t\gamma(\nu+W(\sigma-t))\,d\sigma\right], & t<\dfrac{\nu}{W},\\ \int_0^{\mu_F}h(\mu-\bar{\mu})p\left(t-\dfrac{\nu}{W},\mu\right)d\mu\exp\left[-\int_0^{\nu/W}\gamma(W\sigma)\,d\sigma\right], & t>\dfrac{\nu}{W}.\end{cases} \tag{3.3}$$

Equations (3.2) and (3.3) include transient solutions for small times t and the general solution for large times. We are particularly interested in the long-term behavior of these equations. With the assumption that t is large, $M(t)$ is found to satisfy

$$\begin{aligned}M(t)&=\int_0^{\nu_F}m(t,\nu)\,d\nu\\ &=\int_0^{\nu_F}\int_0^{\mu_F}h(\mu-\bar{\mu})p\left(t-\frac{\nu}{W},\mu\right)d\mu\exp\left[-\int_0^{\nu/W}\gamma(W\sigma)\,d\sigma\right]d\nu.\end{aligned} \tag{3.4}$$

By (3.2) with $(t,\mu)\in S_2$, it is seen that the precursor population p depends only on the hormone level E. Since M depends only on p, as

seen in (3.4), it follows that M is a function of E. Thus, (2.6) and (3.4) form a system of integrodifferential equations or threshold-type delay equations, with the state-dependent delay τ defined implicitly by (3.1).

4. THE MODEL WITH TWO DISCRETE DELAYS AND ITS CHARACTERISTIC EQUATION

The previous section provides a general model for erythropoiesis. However, it includes some unknown functions and an implicitly determined state-dependent time delay, which makes analysis of the system complicated. Using known properties of the erythropoietic system, we introduce several simplifying assumptions that reduce the mathematical complexity of the problem to a mathematical model for erythropoiesis with two discrete time delays. This system of equations has a unique equilibrium about which a linear stability analysis can be performed.

Hematopoietic systems change the velocity of maturation of precursor cells in response to varying physiological conditions. For example, after a severe hemorrhage the oxygen-carrying capacity of the blood decreases significantly, or following a large increase in elevation the inspired oxygen levels are low, leading to a decrease in arterial oxygen. In response, the concentration of Epo increases. This results in elevated stem cell and BFU-E proliferation to produce additional erythrocytes. Furthermore, the maturation transit time from BFU-Es to mature erythrocytes seems to drop from about 7 days to 5 or 6 days. However, the data are arguable, and the variation in the duration of maturation may not be very significant. Thus, as a first approximation we take the maturing velocities as constant and normalize them with time to yield

$$V(E) = 1 \qquad \text{and} \qquad W = 1.$$

With this assumption, (3.1) reduces to $\tau = \mu$.

The general model for erythropoiesis contains a birth rate $\beta(\mu, E)$ dependent on the maturity of the precursor cell and the Epo level. It is known that the precursor cells undergo a series of cell divisions with a generation time of approximately 8 h until they become reticulocytes, at which point the cells stop dividing and simply increase their level of hemoglobin (a measure of maturity). The dependence of β on E is more complicated as Epo appears to affect each of the early stages in different ways. To simplify our model we assume that any increased proliferation of precursor cells is reflected in the number of cells recruited at the boundary. This amounts to letting S_0 depend on E but not β. There is evidence that $S_0(E)$ is a linear function over a range of Epo levels [49]. Another assumption is that the cell generation times for the rapidly proliferating erythroblasts are constant up to a specific

maturity level μ_1, at which point all cell divisions stop. Thus, we take

$$\beta(\mu, E) = \begin{cases} \beta, & \mu < \mu_1, \\ 0, & \mu \geq \mu_1. \end{cases} \tag{4.1}$$

The maturation of the precursor cells in (2.3), which also enter into the boundary conditions (2.1), has a general distribution $h(\mu - \bar{\mu})$ that reflects a range of the age-structured precursor cells that enter the mature population. This corresponds to the variation in hemoglobin content of different red blood cells released into the bloodstream. We simplify the model by assuming that $h(\mu - \bar{\mu})$ is a Dirac δ function with $\bar{\mu} = \mu_F$, that is, all cells are assumed to mature at a specific level of the maturity variable μ. With this assumption and β defined by (4.1), we can solve (3.2) for large time to obtain

$$p(t, \mu) = S_0(E(t - \mu)) \begin{cases} e^{\beta\mu}, & \mu < \mu_1, \\ e^{\beta\mu_1}, & \mu \geq \mu_1. \end{cases}$$

If we write T_1 for μ_F, then it follows that

$$\int_0^{\mu_F} h(\mu - \bar{\mu}) p(t - \nu, \mu) d\mu = S_0(E(t - \nu - T_1)) e^{\beta\mu_1}. \tag{4.2}$$

In (2.4), the death rate γ is assumed to depend on the age of the cell. There are a certain number of erythrocytes lost from all age classes due to leakage of the capillaries and other circulatory damage. Most red blood cells live about 120 days and then are actively degraded due to loss of pliability of the cell membrane. To simplify the model we assume that γ is a small constant for $0 \leq \nu \leq \nu_F$, then becomes infinite at $\nu_F = 120$ days, corresponding to all remaining cells dying at that age. With (4.2) substituted into (3.4), differentiating $M(t)$ gives the following system of equations in the variables M and E:

$$\frac{dM(t)}{dt} = e^{\beta\mu_1}\left[S_0(E(t - T_1)) - e^{-\gamma T_2} S_0(E(t - T_1 - T_2))\right] - \gamma M(t), \tag{4.3a}$$

$$\frac{dE(t)}{dt} = f(M(t)) - kE(t), \tag{4.3b}$$

where ν_F, the maximum age of the mature cell, is written as T_2. Equations (4.3) constitute a nonlinear system of differential equations with two discrete time delays that account for the time required for a

cell to mature in each of the subpopulations. Since the half-life for the hormone Epo is only a few hours, which is short compared to the remaining dynamic time scales in the system, a quasi-steady-state approximation can be applied to Equation (4.3b). This modeling approximation implies that $E = f(M)/k$. The result is a delay differential equation for the mature cells, given by

$$\frac{dM(t)}{dt} = e^{\beta\mu_1}\left[S_1(M(t-T_1)) - e^{-\gamma T_2}S_1(M(t-T_1-T_2))\right] - \gamma M(t), \tag{4.4}$$

where the function $S_1(M) = S_0(f(M)/k)$ incorporates the juxtaposition of the two feedbacks of system (4.3). This system has been examined as a model for platelet control [28, 50, 51]. Despite the many similarities between erythropoiesis and thrombopoiesis, more data are available for the former control system. Our analysis in this paper concentrates on system (4.3) using erythropoiesis, although analogous techniques could be employed in the bifurcation analyses of (4.3) and (4.4).

From the experiments of Clarke and Housman [49], the function $S_0(E)$ is approximately linear in E for a range of Epo levels. When E is sufficiently high, S_0 saturates and even declines slightly. We assume that in the physiological range for normal humans, this control does not saturate because increasing Epo levels result in increased production of erythrocytes. For our analysis, we assume that $S_0(E)$ is an increasing function in E with $S_0(0) = 0$. For a given level of oxygen respiration, the renal cells that sense oxygen concentration release less Epo when oxygen levels increase. When the environmental oxygen is held constant, an increase in oxygen sensed by the renal cells corresponds to increased numbers of erythrocytes or M. Thus, $f(M)$ is a decreasing function with $f(0) > 0$ and $\lim_{M\to\infty} f(M) = 0$.

With these assumptions, Equations (4.3) have a unique equilibrium $(\bar{M}, \bar{E})$. If we define $\bar{S}_0 = e^{\beta\mu_1}S_0'(\bar{E})$, then the characteristic equation for the linearization of system (4.3) about $(\bar{M}, \bar{E})$ is given by

$$\det\begin{vmatrix} \lambda+\gamma & -\bar{S}_0\left(e^{-\lambda T_1} - e^{-\gamma T_2}e^{-\lambda(T_1+T_2)}\right) \\ -f'(\bar{M}) & \lambda + k \end{vmatrix} = 0,$$

which can be written

$$(\lambda+\gamma)(\lambda+k) = -\bar{A}\left(e^{-\lambda T_1} - e^{-\gamma T_2}e^{-\lambda(T_1+T_2)}\right), \tag{4.5}$$

where $\bar{A} \equiv -f'(\bar{M})\bar{S}_0 > 0$. In Section 6 we use this characteristic equation to study the local stability of the equilibrium.

5. PARAMETER ESTIMATION AND SIMULATION OF THE MODEL FOR A NORMAL SUBJECT

Before performing a local stability analysis of the model given in (4.3), we examine the physiological parameters of the system and show a simulation for a normal human subject. With a nonlinearity as given by (2.7), the simplified model given by the system of equations (4.3) contains eight parameters. Few studies show data on the number of erythrocytes and erythropoietin for extended periods of time [52], so we compiled a collection of data from the clinical literature to estimate appropriate values for these parameters. The primary sources for our data are selected chapters (and references therein) from the treatise edited by Williams [37], but even here we noted changes between the third and fourth editions with changes in experimental technology. From these biologically relevant parameter values, we numerically analyze the stability of the equilibrium and determine physiological conditions when instabilities can arise via a Hopf bifurcation.

As a first step, we gather values of the total number of erythrocytes and level of erythropoietin for a normal human subject. This provides the values for the equilibrium point $(\bar{M}, \bar{E})$. The mean number of red blood cells in a normal individual is $\bar{M} = 3.5 \times 10^{11}$ erythrocytes per kilogram of body weight [53]. The normal level of Epo has been reported to be about 10–25 mU/mL [54], although a wide range of values (from 3 to 18,000) have been observed, depending upon the conditions of individuals. Previous estimates obtained with different technology ranged from 6 to 16 (as cited in [55]). With this wide range of Epo concentration we took $\bar{E} = 10$ mU/mL.

Next we consider the values of the delays, T_1 and T_2, representing the length of time for the progenitor cells to mature and the lifespan of the erythrocytes, respectively. The time required for progenitor cells to mature in the bone marrow lies between 5 and 9 days [56]. For our model we have chosen $T_1 = 6$ days. The lifespan of erythrocytes in humans is 120 days [57], which we take for the value of our second delay T_2.

The decay rate γ in (4.3) represents the random destruction of erythrocytes. For normal humans, there is a small loss of 0.06–0.4% per day [57]. Thus, we chose $\gamma = 0.001$ day^{-1}, which corresponds to a loss of approximately 0.1% per day. However, in certain hemolytic anemias there can be a large autoimmune response to the erythrocytes. In Section 6 we will examine what happens to the behavior of the system when this parameter γ is varied.

The half-life for *recombinant* erythropoietin is reported to be 5–6 h [53]. In the third edition of Williams [37], Erslev claims that the half-life

of Epo is 1–2 days. Using the 6-h estimate, we chose $k = 2.8\ \text{day}^{-1}$ for the destruction rate of erythropoietin. Flaharty et al. [56] showed that as the dose of human recombinant Epo changed in normal subjects, there was a significant variation in the measured value for the half-life of erythropoietin. Thus, the underlying assumption of a linear destruction rate in our model is probably too simplistic.

The dependence of the number of cells recruited into the proliferating precursor population is represented by the function $S_0(E)$. As noted earlier, the experiments of Clarke and Housman [49] on the number of BFU-E-derived colonies as a function of Epo give a linear relationship over the normal physiological range, although few data points are presented in this range. Here, we assume that $S_0(E)$ is linear, with slope S_0'. From (4.3), we need to estimate $\bar{S}_0 = e^{\beta\mu_1} S_0'$, where the factor $e^{\beta\mu_1}$ represents the number of reticulocytes formed from one cell recruited into the proliferating precursor population. Under steady-state conditions, $\dot{M} = 0$ implies

$$\bar{S}_0 = \frac{\gamma \bar{M}}{\bar{E}(1 - e^{-\gamma T_2})}. \tag{5.1}$$

From the parameters listed above, this corresponds to $\bar{S}_0 = 0.0031$ ($\times 10^{11}$ erythrocytes/kg body wt)(mL plasma/mU Epo)(day^{-1}).

The most difficult problem we encountered was to find appropriate data to determine the parameters in the nonlinear function $f(M)$. We assumed that $f(M)$ is a Hill function of the form of (2.7) with three defining parameters, a, K, and τ. The data presented in Figure 4 of Erslev [54] shows the logarithm of the concentration of Epo as a function of the percentage of hematocrit for both normal and anemic patients. He provides a straight line as best fit to his semilogarithmic plot of data, and we obtained our values from that line. We assume that the number of erythrocytes is proportional to the percentage of hematocrit. Thus, the normal level of erythropoietin, 10 mU/mL, associated with a level of erythrocytes of 3.5×10^{11} corresponds to a percentage of hematocrit of 43%. We use Erslev's graph to obtain steady-state values of $M = 3.5$, 2.5, and 1.667 ($\times 10^{11}$ erythrocytes/kg body wt) when the concentration of Epo is at 10, 100, and 1000 (mU/mL of plasma), respectively. This yields the three equations $f(3.5) = 2.8 \times 10$, $f(2.5) = 2.8 \times 100$, and $f(1.667) = 2.8 \times 1000$, which can be solved simultaneously by eliminating first a, then K to obtain the set of equations

$$\begin{aligned} (3.5)^\tau - 11(2.5)^\tau + 10(1.667)^\tau &= 0, \\ K\left[(3.5)^\tau - 10(2.5)^\tau\right] &= 9, \\ 28\left[1 + K(3.5)^\tau\right] &= a. \end{aligned}$$

The first equation has a unique positive solution r, with a numerical value of approximately 6.96. Solving the second and third equations for K and a yields successively $K = 0.0382$ and $a = 6570$.

With the above parameters, we simulate the model given by (4.3). Initial data for $t < 0$ were taken to be the equilibrium $(\bar{M}, \bar{E})$, and $M(0) = 0.95\bar{M}$ with $E(0) = \bar{E}$. These initial data represent a normal human who at time $t = 0$ loses 5% of his blood, as would happen in a blood donation. Figure 4 shows the result of the numerical integration. The level of both erythrocytes and erythropoietin show a damped oscillatory return to normal levels. The figure shows that Epo achieves a maximum 3 days after the blood donation with an increase of 42.4% above normal levels. It takes 18 days for the erythrocyte population to return to 99% of the normal level. After 38 days the erythrocyte population exceeds its equilibrium value, but the strong damping makes this barely visible. The results of Maeda et al. [52] of normal subjects after a phlebotomy show a similar response for the 56 days of the experiment. However, the Epo concentration peaks several days later with a more gradual return to normal levels, suggesting more complex physiological controls than our simplified model. They measured hemoglobin concentrations rather than erythrocyte populations, so with hy-

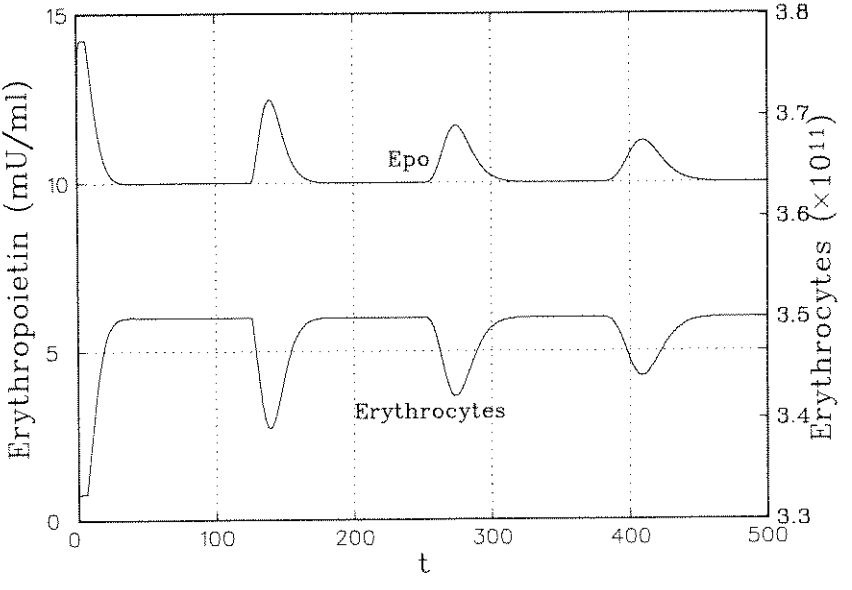

FIG. 4. Numerical integration of Equations (4.3) using normal values of the parameters.

dration after the phlebotomy the hematocrit continued to drop for the first few days.

In the simulation the increased production of erythrocytes after the hypothetical blood donation, however, results in a large population of erythrocytes that die 120 days later due to our assumption on the maximum age of erythrocytes. Thus, there is another response occurring after 126 days due to the delays in the system. In fact, the next maximum Epo concentration and minimum number of erythrocytes occur 139 days into the simulation, with an increase of 24.6% and decrease of 3.14%, respectively. The graph shows further damped responses due to the initial perturbation with the maximum Epo concentrations occurring again at 274 days and 410 days. Clearly, normal individuals would better regulate their erythrocyte production such that these oscillatory responses would be much more damped. An improved model would reflect this if, for example, more general distributions (than a Dirac δ function) were used for the maturing of reticulocytes and the death of erythrocytes.

6. BIFURCATION ANALYSIS AND SIMULATION OF AN AUTOIMMUNE INDUCED HEMOLYTIC ANEMIA

In this section, we examine how the model given by (4.3) can reproduce certain erythropoietic abnormalities. The experiments of Orr et al. [55] produced autoimmune induced hemolytic anemia in rabbits by administration of an incompatible red cell isoantibody. Their experimental results exhibited periodic oscillations in the erythrocyte populations with a mean period of 18 days. Mackey [24, 26] studied the bifurcation problem for the simpler model given by (4.4) for some ranges of the parameters. We now show that our model undergoes a Hopf bifurcation as the destruction rate γ is increased (as the experiment does with the isoantibody) and use this information to demonstrate how well our model agrees with the experimental results. We begin with the bifurcation analysis, then later estimate parameters and simulate the system of delay differential equations for a case of autoimmune induced hemolytic anemia.

From the theory of delay differential equations, the equilibrium solution of (4.3) is asymptotically stable if and only if all solutions λ of (4.5) have negative real parts [58]. Loss of stability of the equilibrium solution of (4.3) occurs via a Hopf bifurcation when a pair of eigenvalues cross the imaginary axis as some parameter in the system is varied. There have been numerous studies for finding purely imaginary eigenvalues for the characteristic equation of a delay differential equation (see, e.g., [59–61]). However, in most studies the delay is one of the

parameters that is varied, while in this problem the delays for the system are known. There have been few bifurcation analyses of delay differential equations with two delays [59, 62], so that provides additional interest to this problem.

The Hopf bifurcation analysis presented here is related to the geometric approach shown in [60, 63, 64]. With $\lambda = i\omega$, we write the characteristic equation as

$$P(\omega)e^{i\theta_1} = -\bar{A}(e^{-i\omega T_1} - e^{-\gamma T_2}e^{-i\omega(T_1+T_2)}) \equiv -\bar{A}Q(\omega), \quad (6.1)$$

where

$$P(\omega) = \left[(\gamma k - \omega^2)^2 + \omega^2(\gamma + k)^2\right]^{1/2}$$

and

$$\theta_1(\omega) = \arctan\left(\frac{\omega(\gamma + k)}{\gamma k - \omega^2}\right)$$

are the magnitude and argument, respectively, of the left-hand side of (6.1). Note that P and θ_1 increase monotonically with ω. Our method for solving (6.1) is to increase ω until the arguments on both sides of the equation agree, then adjust $\bar{A}$ so their magnitudes are equal.

The bifurcation analysis uses the parameter $\bar{A}$, which combines information on the unknown production functions, and γ, which is the destruction rate of mature cells. To find where a Hopf bifurcation occurs, we fix γ and determine the smallest value of $\bar{A}$ that satisfies (6.1) with $\lambda = i\omega$. Figure 5 presents a geometric interpretation of the procedure for determining the Hopf bifurcation. As noted above, P and θ_1 increase monotonically as ω increases with $\lim_{\omega\to\infty}\theta_1(\omega) = \pi$. This creates the parabolic arc seen in the first and second quadrants. The first term in $Q(\omega)$ generates a unit circle in the clockwise direction with increasing ω. The second term in Q is multiplied by $e^{-\gamma T_2}$, so it is thought of as a perturbation. Thus, a first alignment of the arguments of the left and right sides of (6.1) occurs for $0 < \omega < \pi/T_1$, where $\theta_1(\omega) = \pi + \arg Q(\omega)$. By taking $\bar{A} = P(\omega)/|Q(\omega)|$, we find where the Hopf bifurcation occurs.

It is the second term in Q, which includes the second delay, that complicates the analysis. If γ is sufficiently large, then this term is only a very small perturbation, and the Hopf bifurcation analysis is similar to a problem with only one delay. However, as γ decreases, the effects from this term become more pronounced, and multiple alignments of the argument can occur for $0 < \omega < \pi/T_1$. The smallest value of $\bar{A}$ is where the Hopf bifurcation occurs.

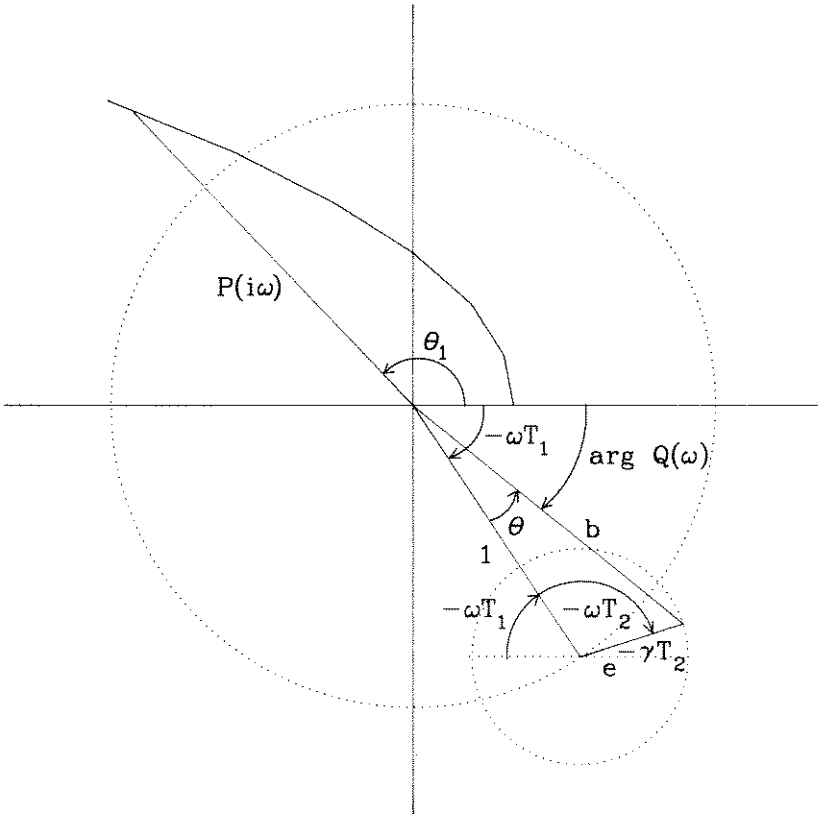

FIG. 5. A geometric interpretation for determining the Hopf bifurcation.

As seen in Figure 5, the second term in Q generates a clockwise circle of radius $e^{-\gamma T_2}$ whose center moves along the unit circle of the first term in Q. The circling of this term is more rapid because of its frequency, $T_1 + T_2$, which allows the multiple alignments. An application of the law of cosines provides the magnitude and argument of Q. Applying this law and referring to Figure 5, we find that if $\alpha \equiv \text{mod}(\omega T_2, 2\pi)$, then

$$b^2 = 1 + e^{-2\gamma T_2} - 2\cos\alpha,$$

$$\cos\theta = \frac{1 - e^{-\gamma T_2}\cos\alpha}{b}.$$

With this information, the argument of the right-hand side for the characteristic equation (6.1) satisfies

$$\arg Q(\omega) = \begin{cases} -\operatorname{mod}(\omega T_1, 2\pi) + \theta, & \alpha < \pi, \\ -\operatorname{mod}(\omega T_1, 2\pi) - \theta, & \alpha > \pi. \end{cases}$$

Thus, for a given set of parameters k, γ, T_1, and T_2, we increase ω and numerically find all solutions to $\theta_1(\omega) = \pi + \arg Q(\omega)$, $0 < \omega < \pi / T_1$. For each of these values of ω, we take $\bar{A} = P(\omega)/b$, which yields a pair of imaginary eigenvalues that solve (4.5) [or (6.1)]. The smallest value of $\bar{A}$, as computed above, is where the equilibrium of (4.3) loses stability from a Hopf bifurcation.

A CASE STUDY OF AUTOIMMUNE INDUCED HEMOLYTIC ANEMIA

In the experiments of Orr et al. [55], rabbits were injected every 2–3 days with an incompatible red cell isoantibody, which produced an autoimmune induced hemolytic anemia. The erythrocyte population in one experimental rabbit (Figure 4 in [55]) fluctuated about 10% above and below the anemic mean of 75% of normal erythrocyte levels. The observed oscillations for this rabbit had a periodicity of 17 days. For our analysis we used their parameter values to test the model given by (4.3).

Orr et al. [55] state that their data indicate the time for precursor cells in the rabbit erythron is about 3 days, so we let $T_1 = 3$ days. Experiments of Burwell et al. [65] give the normal erythrocyte lifespan to be 45–50 days, so we took $T_2 = 50$ days. The half-life of circulating erythropoietin in rats is about 2.5 h (as cited in [55]), so using this estimate for rabbits we took $k = 6.65$ day^{-1}.

The parameters in the nonlinear function were determined from the data in Erslev [54], so we used the human data quoted before for the equilibrium $(\bar{M}, \bar{E})$. Thus, 75% of normal gives $\bar{M} = 2.63$ ($\times 10^{11}$ erythrocytes/kg body wt). From these data we obtain $\bar{E} = 71.1$ (mU/mL plasma). With the information above, the parameter values in the nonlinear function can be computed. The values for r and K do not change from the values for a normal human subject, so again we let $r = 6.96$ and $K = 0.0382$. The smaller half-life of Epo (k) affects the value of a, giving $a = 15{,}600$. For the bifurcation analysis we need $f'(\bar{M})$, which satisfies

$$f'(\bar{M}) = -\frac{aKr\bar{M}^{r-1}}{(1 + K\bar{M}^r)^2} \simeq -1210.$$

The quantities that we consider unknown are the destruction rate of erythrocytes, γ, and the production of erythrocytes, $S_0(E)$. In the previous section we assumed $S_0(E)$ linear and showed that under steady-state conditions $\bar{S}_0$ given by (5.1) represented the rate of production of erythrocytes per day per milliunit of erythropoietin. Thus, for a given $(\bar{M}, \bar{E})$ and T_2, $\bar{S}_0$ is a function depending on γ. The bifurcation analysis presented above uses the parameter $\bar{A}$, which in Section 4 is given by $\bar{A} = -f'(\bar{M})\bar{S}_0$.

From the data above we develop the stability diagram presented in Figure 6. As γ varies, our calculations of $\bar{A}$ for the model at equilibrium with 75% of the normal hemoglobin produces the curve labeled Model (Equilibrium). The remaining lines in the diagram show the solutions of (6.1) as γ varies. From our discussion above, we fix a value of γ, then compute all values $0 < \omega < \pi / T_1$, where the arguments of the right- and left-hand sides of (6.1) agree and adjust the value of $\bar{A}$ so that the magnitudes agree. This gives the purely imaginary eigenvalues to the linearized model (4.3) where a possible Hopf bifurcation can occur.

When $\bar{A}$ is larger than the smallest value of $\bar{A}$ that solves (6.1) for a given γ, the equilibrium of the linearization of (4.3) becomes unstable

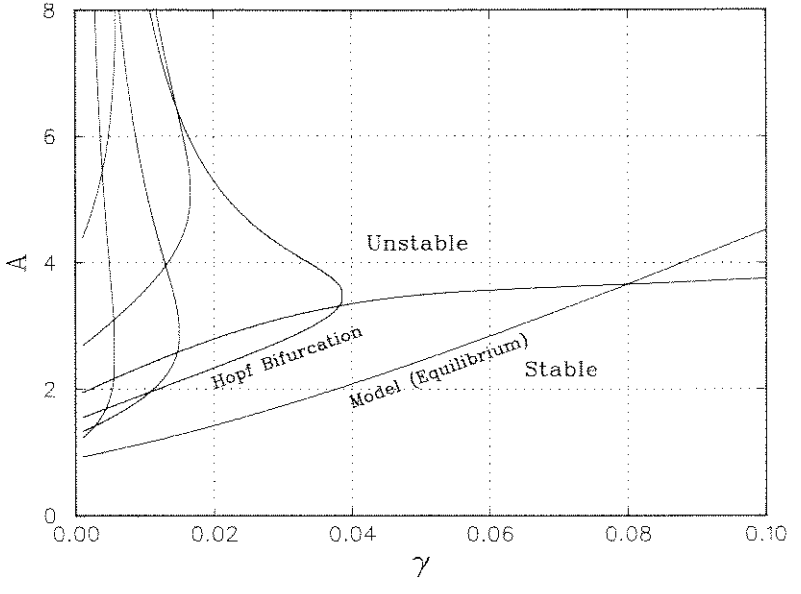

FIG. 6. Stability diagram for determining where a Hopf bifurcation occurs in Equation (4.4), using Equation (4.5).

as labeled in Figure 6. This result is easily shown using the argument principle [60]. Note that this may not be the smallest value of ω that solves (6.1). The bifurcation diagram shows that this two-delay problem becomes very complicated as γ decreases. As noted above, multiple alignments occur for small values of γ when $0 < \omega < \pi / T_1$, which means that several values of $\bar{A}$ must be computed to determine where stability is lost.

From Figure 6 we see that near $\gamma = 0.08$ the erythropoiesis model (4.3) with the calculated parameters undergoes a Hopf bifurcation. Thus, as the destruction rate γ rises above this critical value, the nonlinear model loses stability and develops oscillatory solutions. At this bifurcation point, $\omega \simeq 0.549$, which corresponds to a period of 11.4 days. This is shorter than the actual observed period, but the sensitivity to the many parameters has not yet been determined to see if this error is acceptable. We note that the lowest bifurcation curve in Figure 6 for $0.003 < \gamma < 0.011$ yields $\omega \simeq 0.345$, which corresponds to a period of about 18 days. Furthermore, the other root crossings nearby could lead to more complicated dynamics [59] as displayed in the experimental data. However, this value of γ is too low to relate to the case of autoimmune induced hemolytic anemia that is being studied here.

Figure 7 presents a numerical simulation of the model given by (4.3) for the case of autoimmune hemolytic anemia in rabbits. For simulation purposes we choose $\gamma = 0.1$. The simulation begins with the rabbits having normal levels of erythrocytes and erythropoietin. We assume that the incompatible red cell isoantibody is injected at $t = 0$ and maintains a constant effect throughout the simulation. (This assumption is more like an intravenous supply of the isoantibody rather than the regular injections given in the experiment.) Orr et al. [55] claim that the isoantibody may selectively kill the oldest cells, resulting in cells living to only 14 days. With our assumption on γ we have a nonselective destruction of erythrocytes causing an exponential loss. The choice of $\gamma = 0.1$ would correspond to half the cells dying by age 7, which is the mean of their choice. By age 14, 75% of the erythrocytes would be destroyed, so our parameter choice is similar to the one they used for their model where there is no cell death until age 14 days, at which point all erythrocytes are destroyed.

As noted before, the simulation in Figure 7 displays oscillations with a period shorter than the experiments. Also, the mean is shifted higher by 5% despite our choice of parameters. The amplitude of the simulation is very similar to the experiments: the lower values of the erythrocytes agree quite well, and the higher values are slightly less than 10% higher than those observed in the experiments. The variation in the concentration of erythropoietin is very dramatic. From the initial nor-

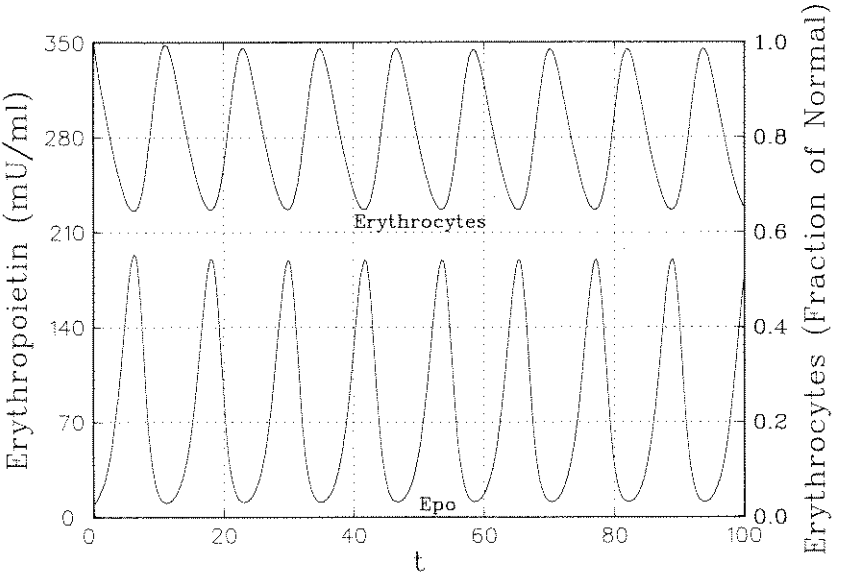

FIG. 7. Simulation of the two-delay model for autoimmune hemolytic anemia in rabbits [Eq. (4.4)].

mal concentration of 10 mU/mL, the autoimmune induced hemolytic anemia causes the erythropoietin level in the model to increase more than 18-fold to concentrations exceeding 180 mU/mL. Thus, we conclude that our model does seem to give the qualitative behavior found in the experiments, but further studies are needed to determine how accurately our choices of parameters reflect the actual process of erythropoiesis.

7. DISCUSSION

As erythrocytes are one of the best understood hematopoietic cell lines, the regulation and control of erythrocyte numbers lends itself naturally to the development of an age-structured model describing the known physiological processes leading to the production of mature red blood cells. We have traced this development here and, using the method of characteristics, have shown how the age-structured model for erythropoiesis leads to a system of threshold-type differential delay equations as a natural consequence of the physiology. Further simplifying assumptions reduced this system to a model with two discrete delays. We carried out the local stability and bifurcation analysis for this system about the steady state and demonstrated once again how compli-

cated two-delay problems can be. Our simulation studies have shown that a perturbation of the erythropoietic system, as would occur in a normal human following a blood donation event, leads to a damped oscillatory return of the system to normal. We feel that the model gives an idealized system in which to explore the dynamics of blood donation regimens, an event that occurs many thousands of times daily worldwide. Another simulation meant to reproduce the consequences of an elevated random peripheral destruction of red blood cells, as would occur in autoimmune hemolytic anemia, clearly demonstrates the existence of sustained oscillations in the number of erythrocytes, as has been noted both experimentally and clinically.

In spite of the physiological realism of our age-structured model, it is also clear that the experimental and clinical data are inadequate to fully define all of the important facets of the model. Thus, for example, more studies are needed on how the model behavior is affected by the poorly understood state-dependent velocity of maturing of precursors. Other factors, such as the role of chalone and iron, need to be examined more closely under stress conditions to determine what the rate-limiting reactions are. Since there are insufficient data to define all of the parameters in our age-structured model, the model must evolve with experimental advances in the future.

Previous studies have considered delay differential equations as models of blood cell populations [26, 28]. In those instances, however, the governing equation contained a single time lag. From a mathematical point of view, there are significant differences in the stability properties of delay differential equations, as the number of time lags is increased from one to two [62]: stability switches can occur, and multiple modes can be destabilized simultaneously. In erythropoiesis, these differences are probably not crucial to the dynamics, since the ratio of the two time delays is quite large (about 20). For other, similar systems, in which this ratio is smaller, for example, in thrombopoiesis, these complications may become biologically relevant.

Indeed, normal mammalian thrombopoiesis is organized and regulated in a similar manner to the erythropoietic process studied here (see [66–68] for more details and references to the literature). In thrombopoiesis, the pluripotential stem cells become committed stem cells, which then form megakaryocytes through a series of biochemical signals that are not fully understood. The maturation of the megakaryocyte differs from that of precursors of erythrocytes in that there is replication and division of the nuclear material with a concomitant increase in cytoplasmic volume. Megakaryocytes produce platelets by first forming intracellular cytoplasmic platelet subunits, which are subsequently released into the circulation as platelets. The total elapsed time between

the appearance of a recognizable megakaryocyte and when it starts to produce platelets is about 9 days in the normal human [69]. Once released into the circulation, platelets normally disappear primarily through senescence, living for approximately 10 days in humans [70]. Platelet production is regulated via the humoral stimulator thrombopoietin, analogous to the regulation of erythropoiesis by erythropoietin.

This indicates that our model for erythropoiesis is also applicable to the regulation of thrombopoiesis with significantly different parameter values. In preliminary studies, we have found that although there are sufficient data to determine many of the parameters for a corresponding thrombopoietic model, the data are inadequate to obtain the nature of the important nonlinear proliferative feedback function corresponding to the function f of Equation (2.7). Some preliminary bifurcation analyses show that the smaller second delay in thrombopoiesis decreases the stability of the model, which suggests that this hematopoietic system is inherently less stable and may be more susceptible to dynamic disorders. The lack of adequate data is unfortunate as there are a number of fascinating and sometimes fatal dynamic oscillatory platelet disorders whose mechanistic origin is obscure [71, 72]. Better understanding of the potential origin of these disorders from a modeling perspective might lead to alternative clinical strategies in dealing with them.

APPENDIX. DETAILS FOR THE METHOD OF CHARACTERISTICS

The method of characteristics is used to simplify the partial differential equations (2.3) and (2.4). Our techniques follow Metz and Diekmann [43] and Smith [48]. For (2.3), we assume a parametrization s in the $t\mu$ space with $t > 0$ and $0 < \mu < \mu_F$. If $P(s) = p(t(s), \mu(s))$, then differentiating with respect to s produces the total derivative of p and yields

$$\frac{dP(s)}{ds} = \frac{d}{ds} p(t, \mu) = \frac{\partial p}{\partial t} \frac{dt}{ds} + \frac{\partial p}{\partial \mu} \frac{d\mu}{ds}.$$

The parameter s follows a characteristic curve for (2.3) provided

$$\frac{dt}{ds} = 1 \qquad \text{and} \qquad \frac{d\mu}{ds} = V(E(t)).$$

Thus, the characteristic curves are given by

$$t(s) - t(0) = s \qquad \text{and} \qquad \mu(s) - \mu(0) = \int_0^s V(E(t(\sigma)))\, d\sigma. \quad \text{(A.1)}$$

Figure 3 shows typical characteristic curves in the $t\mu$ plane. This figure shows how the characteristic curve C_0 that emanates from the point $(t(0), \mu(0)) = (0,0)$ separates the $t\mu$ space into the two regions S_1 and S_2 as discussed in Section 3.

Along these characteristics, if (2.3) is written as

$$\frac{dP}{ds} = F(t(s), \mu(s))P,$$

where $F(t, \mu) = \beta(\mu, E(t)) - V(E(t))H(\mu)$, then the solution is given by

$$P(s) = P(0)\exp\left[\int_0^s F(t(w), \mu(w))\,dw\right]. \tag{A.2}$$

The solution to (A.2) has a different form in each of the regions S_1 and S_2.

For S_1, $t(s) = s$ and $\mu(s) = \mu(0) + \int_0^s V(E(\sigma))d\sigma$ with $0 < \mu(0) < \mu_F$. Thus,

$$\mu(0) = \mu - \int_0^t V(E(\sigma))\,d\sigma \qquad \text{and} \qquad \mu(w) = \mu - \int_w^t V(E(\sigma))\,d\sigma.$$

If we assume that the initial age structure of the precursor population satisfies

$$p(0, \mu) = \phi(\mu),$$

then $P(0) = p(0, \mu(0)) = \phi(\mu(0))$. From this information and (A.2), we find that for $(t, \mu) \in S_1$,

$$\begin{aligned} P(s) &= p(t, \mu) \\ &= \phi\left(\mu - \int_0^t V(E(\tau))\,d\tau\right)\exp\left[\int_0^t F\left(w, \mu - \int_w^t V(E(\tau))\,d\tau\right)dw\right]. \end{aligned}$$

For solutions in S_2, the characteristic curve intersects the t axis with $\mu(0) = 0$. From (A.1) it follows that

$$\begin{aligned} \mu(s) &= \int_0^s V(E(t(\sigma)))\,d\sigma = \int_0^s V(E(\sigma + t(0)))\,d\sigma \\ &= \int_{t(0)}^{t(0)+s} V(E(w))\,dw. \end{aligned}$$

Let (t, μ) be an arbitrary point in S_2 with $0 < \mu < \mu_F$. If τ is the time required for the maturation level to increase from 0 to μ, it follows that τ is an implicitly defined variable that depends on the state of the system and is given by

$$\mu = \int_{t-\tau}^{t} V(E(w))\,dw. \tag{A.3}$$

Once τ is determined from (A.3), then $t(0) = t - \tau$ and $P(0) = p(t(0),0) = p(t-\tau,0)$. The boundary condition (2.1) gives $p(t,0) = S_0(E)/V(E)$. Substituting this information into (A.2) gives

$$P(s) = p(t,\mu) = p(t-\tau,0)\exp\left[\int_0^s F(w + t(0), \mu(w))\,dw\right]$$

$$= \frac{S_0(E(t-\tau))}{V(E(t-\tau))}\exp\left[\int_{t-\tau}^{t} F\left(\sigma, \int_{t-\tau}^{\sigma} V(E(\tau))\,d\tau\right)d\sigma\right].$$

This work was supported in part by NSF grants DMS-9007718 and DMS-9208290 (to JMM), by NSERC, FCAR, and NATO grants (to JB and MCM), and by the Alexander von Humboldt Stiftung (MCM). Part of this work was performed when JMM was visiting the Centre de Recherches Mathématiques and Centre for Nonlinear Dynamics in Montréal.

We dedicate this work to the memory of Stavros Busenberg, a consumate applied mathematician who affected all of us in different, but profound, ways.

REFERENCES

1 H. A. Reimann, *Periodic Diseases*, F. A. Davis, Philadelphia, 1963.
2 M. C. Mackey and L. Glass, Oscillation and chaos in physiological control systems, *Science* 197:287–289 (1977).
3 L. Glass and M. C. Mackey, *From Clocks to Chaos: The Rhythms of Life*, Princeton Univ. Press, Princeton, NJ, 1988.
4 L. Glass, C. Graves, G. A. Petrillo, and M. C. Mackey, Unstable dynamics of a periodically driven oscillator in the presence of noise, *J. Theor. Biol.* 86:455–476 (1980).
5 U. an der Heiden, M. C. Mackey, and H. O. Walther, Complex oscillations in a simple deterministic neuronal network, in *Mathematical Aspects of Physiology*, F. C. Hoppensteadt, Ed., American Mathematical Society, Providence, RI, 1981, pp. 355–360.
6 L. K. Kaczmarek, A model of cell firing patterns during epileptic seizures, *Biol. Cybern.* 22:229–234 (1976).

7 L. K. Kaczmarek and A. Babloyantz, Spatiotemporal patterns in epileptic seizures, *Biol. Cybern.* 26:199–208 (1977).
8 A. Longtin, J. G. Milton, J. E. Bos, and M. C. Mackey, Noise and critical behaviour of the pupil light reflex at oscillation onset, *Phys. Rev.* Phys. Rev. A 41:6992–7005 (1990).
9 M. C. Mackey and U. an der Heiden, The dynamics of recurrent inhibition, *J. Math. Biol.* 19:211–225 (1984).
10 J. G. Milton, A. Longtin, A. Beuter, M. C. Mackey, and L. Glass, Complex dynamics and bifurcations in neurology, *J. Theor. Biol.* 138:129–147 (1989).
11 D. R. Adam, J. M. Smith, S. Askelron, S. Nyberg, A. O. Powell, and R. J. Cohen, Fluctuations in T-wave morphology and susceptibility to ventricular fibrillation, *J. Electrocard.* 17:209–218 (1984).
12 T. R. Chay and Y. S. Lee, Impulse responses of automaticity in the Purkinje fiber, *Biophys. J.* 45:841–849 (1984).
13 R. J. Cohen and R. D. Berger, A quantitative model for ventricular response during atrial fibrillation, *IEEE Trans. Biomed.* BME30:769–781 (1983).
14 L. Glass, M. R. Guevara, A. Shrier, and R. Perez, Bifurcation and chaos in a periodically stimulated cardiac oscillator, *Physica* 7D:89–101 (1983).
15 M. R. Guevara and L. Glass, Phase locking, period doubling bifurcations and chaos in a mathematical model of a periodically driven oscillator: a theory for the entrainment of biological oscillators and the generation of cardiac dysrhythmias, *J. Math. Biol.* 14:1–24 (1982).
16 M. R. Guevara, L. Glass, M. C. Mackey, and A. Shrier, Chaos in neurobiology, *IEEE Trans. Syst., Man Cybern.* SMC-13:790–798 (1983).
17 M. R. Guevara, L. Glass, and A. Shrier, Phase locking, period-doubling bifurcations, and irregular dynamics in periodically stimulated cardiac cells, *Science* 214:1350–1353 (1981).
18 J. P. Keener, Chaotic cardiac dynamics, in *Mathematical Aspects of Physiology*, F. C. Hoppensteadt, Ed., American Mathematical Society, Providence, RI, 1981, pp. 299–325.
19 J. P. Keener, On cardiac arrhythmias: AV conduction block, *J. Math. Biol.* 12:215–225 (1981).
20 A. L. Ritzenberg, D. R. Adam, and R. J. Cohen, Period multiplying: evidence for nonlinear behavior in the canine heart, *Nature* 307:159–161 (1984).
21 A. L. Ritzenberg, J. M. Smith, M. P. Grumbach, and R. J. Cohen, Precursor to fibrillation in a cardiac computer model, in *IEEE Computers in Cardiology*, IEEE Computer Society Press, Silver Spring, MD, 1984, pp. 171–174.
22 J. M. Smith and R. J. Cohen, Simple finite-element model accounts for wide range of cardiac dysrhythmias, *Proc. Natl. Acad. Sci. U.S.A.* 81:233–237 (1984).
23 A. Lasota, M. C. Mackey, and M. Wazewska-Czyzewska, Minimizing therapeutically induced anemia, *J. Math. Biol.* 13:149–158 (1981).
24 M. C. Mackey, A unified hypothesis for the origin of aplastic anemia and periodic haematopoiesis, *Blood* 51:941–956 (1978).
25 M. C. Mackey, Dynamic haematological disorders of stem cell origin, in *Biophysical and Biochemical Information Transfer in Recognition*, J. G. Vassileva-Popova and E. V. Jensen, Eds., Plenum, New York, 1979, pp. 373–409.
26 M. C. Mackey, Periodic auto-immune hemolytic anemia: an induced dynamical disease, *Bull. Math. Biol.* 41:829–834 (1979).

27 M. C. Mackey, Some models in hemopoiesis: predictions and problems, in *Biomathematics and Cell Kinetics*, M. Rotenberg, Ed., Elsevier/North Holland, New York, 1981, pp. 23–38.
28 M. C. Mackey and J. G. Milton, Feedback, delays and the origin of blood cell dynamics, *Comments Theor. Biol.* 1:299–327 (1990).
29 J. G. Milton and M. C. Mackey, Periodic haematological diseases: mystical entities or dynamical disorders?, *J. Roy. Coll. Physicians Lond.* 23:236–241 (1989).
30 A. Morley, Cyclic hemopoiesis and feedback control, *Blood Cells* 5:283–296 (1979).
31 J. Cronin-Scanlon, A mathematical model for catatonic schizophrenia, *Ann. N.Y. Acad. Sci.* 231:112–122 (1974).
32 R. King, J. D. Barchas, and B. A. Huberman, Chaotic behavior in dopamine neurodynamics, *Proc. Natl. Acad. Sci. U.S.A.* 81:1244–1247 (1984).
33 L. Glass and M. C. Mackey, Pathological conditions resulting from instabilities in physiological control systems, *Ann. N.Y. Acad. Sci.* 316:214–235 (1979).
34 M. C. Mackey and U. an der Heiden, Dynamical diseases and bifurcations: understanding functional disorders in physiological systems, *Funkt. Biol. Med.* 1:156–164 (1982).
35 M. C. Mackey and J. G. Milton, Dynamical diseases, *Ann. N.Y. Acad. Sci.* 504:16–32 (1986).
36 L. Rensing, U. an der Heiden, and M. C. Mackey, *Temporal Disorder in Human Oscillatory Systems*, Springer-Verlag, New York, 1987.
37 M. M. Williams, *Hematology*, 4th ed., McGraw-Hill, New York, 1990.
38 S. Busenberg, K. Cooke, and M. Iannelli, Endemic thresholds and stability in a class of age-structured epidemics, *SIAM J. Appl. Math.* 48:1379–1395 (1988).
39 S. Busenberg and M. Iannelli, Separable models in age-dependent population dynamics, *J. Math. Biol.* 22:145–173 (1985).
40 O. Diekmann and J. A. J. Metz, On the reciprocal relationship between life histories and population dynamics, in *Frontiers in Theoretical Biology* (Lect. Notes Biomath. 100), S. A. Levin, Ed., Springer-Verlag, New York, 1994, pp. 19–22.
41 A. Grabosch and H. J. A. M. Heijmans, Cauchy problems with state-dependent time evolution, *Jn. J. Appl. Math.* 7:433–457 (1990).
42 A. Grabosch and H. J. A. M. Heijmans, Production development and maturation of red blood cells. A mathematical model, in *Mathematical Population Dynamics*, D. E. Axelrod, O. Arino, and M. Kimmel, Eds., Marcel Dekker, New York, 1991, pp. 189–210.
43 J. A. J. Metz and O. Diekmann, *The Dynamics of Physiologically Structured Populations* (Lect. Notes Biomath. 68), Springer-Verlag, Berlin, 1986.
44 G. Webb, Random transitions, size control, and inheritance in cell population dynamics, *Math. Biosci.* 84:1–21 (1987).
45 M. C. Mackey and P. Dörmer, Continuous maturation of proliferating erythroid precursors, *Cell Tissue Kinet.* 15:381–392 (1982).
46 J. A. Gatica and P. Waltman, A threshold model of antigen antibody dynamics with fading memory, in *Nonlinear Phenomena in Mathematical Sciences*, V. Lakshmikantham, Ed., Academic, New York, 1982.
47 J. A. Gatica and P. Waltman, A system of functional differential equations modeling threshold phenomena, *Appl. Anal.* 28:39–50 (1988).

48 H. L. Smith, Reduction of structured population models to threshold-type delay equations and functional differential equations: a case study, *Math. Biosci.* 113:1–23 (1993).
49 B. J. Clarke and D. Housman, Characterisation of an erythroid precursor cell of high proliferative capacity in normal human peripheral blood, *Proc. Natl. Acad. Sci. U.S.A.* 74:1105–1109 (1977).
50 J. Bélair, Bifurcations in a model of the platelet regulatory system, in *Chaos in Biological Systems*, A. Degn, A. V. Holden, and L. F. Olsen, Eds., Plenum, New York, 1987, pp. 19–22.
51 J. Bélair and M. C. Mackey, A model for the regulation of mammalian platelet production, *Ann. N.Y. Acad. Sci.* 504:280–282 (1987).
52 H. Maeda, Y. Hitomi, R. Hirata, H. Tohyama, J. Suwata, S. Kamata, Y. Fujino, and N. Murata, The effect of phlebotomy on serum erythropoietin levels in normal healthy subjects, *Int. J. Hematol.* 55:111–115 (1992).
53 A. J. Erslev, Production of erythrocytes, in *Hematalogy*, M. M. Williams, Ed., McGraw-Hill, New York, 1990, pp. 389–397.
54 A. J. Erslev, Erythropoietin titers in health and disease, *Semin. Hematol.* 28 (Suppl. 3):2–8 (1991).
55 J. S. Orr, J. Kirk, K. G. Gray, and J. R. Anderson, A study of the interdependence of red cell and bone marrow stem cell populations, *Br. J. Haematol.* 15:23–34 (1968).
56 K. K. Flaharty, J. Cairo, A. Erslev, J. J. Whalen, E. M. Morris, T. D. Bjornsson, and P. H. Vlasses, Pharmacokinetics and erythropoietic response to human recombinant erythropoietin in healthy men, *Clin. Pharmacol. Ther.* 47:557–564 (1990).
57 A. J. Erslev, Erythrokinetics, in *Hematalogy*, M. M. Williams, Ed., McGraw-Hill, New York, 1990, pp. 414–442.
58 J. K. Hale, *Theory of Functional Differential Equations*, Springer-Verlag, New York, 1977.
59 J. Bélair and S. A. Campbell, Stability and bifurcations of equilibria in a multiple-delayed differential equation, *SIAM J. Appl. Math.* 54:1402–1424 (1994).
60 J. M. Mahaffy, A test for stability of linear differential delay equations, *Quart. Appl. Math.* 40:193–202 (1982).
61 J. M. Mahaffy, Stability of periodic solutions for a model of genetic repression with delays, *J. Math. Biol.* 22:137–144 (1985).
62 J. M. Mahaffy, P. J. Zak, and K. M. Joiner, A geometric analysis of the stability regions for a linear differential equation with two delays, Int. J. Bifur. Chaos, in press (1995).
63 S. N. Busenberg and J. M. Mahaffy, The effects of dimension and size for a compartmental model of repression, *SIAM J. Appl. Math.* 48:882–903 (1988).
64 S. N. Busenberg and J. M. Mahaffy, A compartmental reaction-diffusion cell cycle model, *Comput. Math. Appl.* 18:883–892 (1989).
65 E. L. Burwell, B. A. Brickley, and C. A. Finch, Erythrocyte life span in small mammals, *Am. J. Physiol.* 172:718 (1953).
66 S. Ebbe and F. Stohlman, Megakaryocytopoiesis in the rat, *Blood* 26:20–35 (1965).
67 L. A. Harker, The kinetics of platelet production and destruction in man, *Clin. Haematol.* 6:671–693 (1977).

68 M. M. Wintrobe, *Clinical Hematology*, 7th ed., Lea and Febiger, Philadelphia, 1976.
69 U. Muller, J. Kulinna, J. Luber, H.-P. Hebestreit, M. Mayer, U. Kempgens, and W. Quisser, *In vivo* study of platelet kinetics by ^{75}Se-methionine in different haematological disorders, *Blut* 34:31–38 (1977).
70 L. A. Harker and C. A. Finch, Thrombokinetics in man, *J. Clin. Invest.* 48:963–974 (1969).
71 I. Branehog, J. Kutti, B. Ridell, B. Swolin, and A. Weinfeld, The relation of thrombokinetics to bone marrow megakaryocytes in idiopathic thrombocytopenic purpura (ITP), *Blood* 45:551–562 (1975).
72 I. Branehog, J. Kutti, and A. Weinfeld, Platelet survival and platelet production in idiopathic thrombocytopenic purpura (ITP), *Br. J. Haematol.* 27:127–143 (1974).